Caged Vanilloid Ligands for Activation of TRPV1 Receptors by 1- and 2-Photon Excitation[†]

Jun Zhao,[‡] Tony D. Gover,[§] Sukumaran Muralidharan,[‡] Darryl A. Auston,[‡,||] Daniel Weinreich,[§,⊥] and Joseph P. Y. Kao*[,‡,§,||]

Medical Biotechnology Center, University of Maryland Biotechnology Institute, Baltimore, Maryland, Program in Neuroscience, University of Maryland, Baltimore, Maryland, Department of Pharmacology, University of Maryland School of Medicine, Baltimore, Maryland, and Department of Physiology, University of Maryland School of Medicine, Baltimore, Maryland

ABSTRACT: Nociceptive neurons in the peripheral nervous system detect noxious stimuli and report the information to the central nervous system. Most nociceptive neurons express the vanilloid receptor, TRPV1, a nonselective cation channel gated by vanilloid ligands such as capsaicin, the pungent essence of chili peppers. Here, we report the synthesis and biological application of two caged vanilloids: biologically inert precursors that, when photolyzed, release bioactive vanilloid ligands. The two caged vanilloids, Nb-VNA and Nv-VNA, are photoreleased with quantum efficiency of 0.13 and 0.041, respectively. Under flash photolysis conditions, photorelease of Nb-VNA and Nv-VNA is 95% complete in ∼40 μs and ∼125 μs, respectively. Through 1-photon excitation with ultraviolet light (360 nm), or 2-photon excitation with red light (720 nm), the caged vanilloids can be photoreleased in situ to activate TRPV1 receptors on nociceptive neurons. The consequent increase in intracellular free Ca^{2+} concentration ($[Ca^{2+}]_i$) can be visualized by laser-scanning confocal imaging of neurons loaded with the fluorescent Ca^{2+} indicator, fluo-3. Stimulation results from TRPV1 receptor activation, because the response is blocked by capsazepine, a selective TRPV1 antagonist. In Ca^{2+}-free extracellular medium, photoreleased vanilloid can still elevate $[Ca^{2+}]_i$, which suggests that TRPV1 receptors also reside on endomembranes in neurons and can mediate Ca^{2+} release from intracellular stores. Notably, whole-cell voltage clamp measurements showed that flash photorelease of vanilloid can activate TRPV1 channels in <4 ms at 22 °C. In combination with 1- or 2-photon excitation, caged vanilloids are a powerful tool for probing morphologically distinct structures of nociceptive sensory neurons with high spatial and temporal precision.

In the peripheral nervous system, nociceptive sensory neurons, or nociceptors, detect noxious stimuli and convert these stimuli into action potentials that are transmitted to the central nervous system (*1*). The vast majority of nociceptive neurons express the vanilloid receptor, TRPV1,[1,2] which is a ligand-gated nonselective cation channel with high permeability to Ca^{2+}, Na^+, and K^+ ions (*2*). Although the endogenous vanilloid ligand is still unknown, a reliable

exogenous ligand for TRPV1 is capsaicin (*3*), the pungent, or "hot", essence of capsicum peppers. Capsaicin (Figure 1) binds TRPV1 and activates the receptor with high potency ($EC_{50} \approx 10^{-7}$ M) (*4*). Activated TRPV1 permits nonselective cation flux into neurons, causing membrane depolarization, which is measurable electrophysiologically, as well as a rise in intracellular free Ca^{2+} concentration ($[Ca^{2+}]_i$), which can be detected quantitatively through the use of fluorescent Ca^{2+} indicators (*5*). Coupled with the above techniques, capsaicin could be used to identify and probe nociceptors in living tissue preparations. Unfortunately, conventional means for delivering capsaicin (e.g., application by bath perfusion or by local perfusion through a puffer pipet) do not have adequate temporal or spatial resolution to permit stimulation of a single cell body or a single nerve terminal in an anatomically complex tissue preparation. In contrast, because light can be focused to a diffraction-limited spot (<1 μm), and photochemical reactions are fast (typically $\ll 1$ ms), focal photolysis of a "caged" molecule—a biologically inert but photolabile precursor—is an ideal way to generate a biological ligand in situ with high spatiotemporal control. Since Kaplan and colleagues first reported the synthesis and biological application of caged ATP (*6*), the field of caged molecules has undergone extensive growth and maturation. Expert reviews of progress in this field have appeared
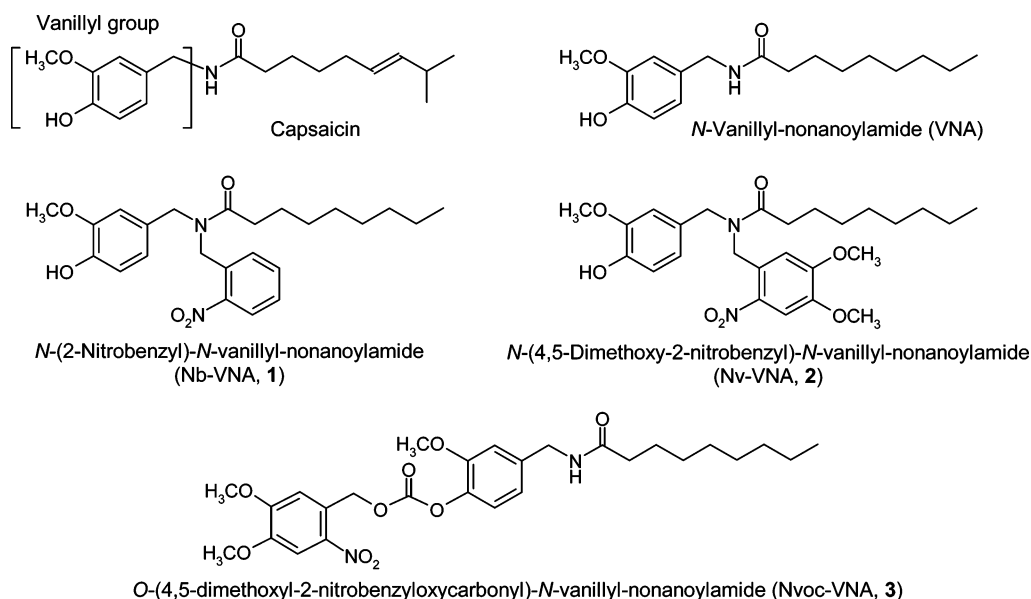
FIGURE 1: Structures of vanilloid molecules. The structures of capsaicin, *N*-vanillylnonanoylamide (VNA), and the nitrobenzyl- (Nb), nitroveratryl- (Nv), and nitroveratryloxycarbonyl- (Nvoc) caged versions of VNA are shown.

regularly (*7−12*). Here we report the design and synthesis of two lipophilic caged vanilloid ligands and demonstrate their utility for rapidly activating TRPV1 receptors on primary sensory neurons by 1- and 2-photon excitation.

MATERIALS AND METHODS

Organic Synthesis

Reagents and solvents for chemical synthesis and chromatography were purchased from commercial vendors (Aldrich, Milwaukee, WI; Fisher Scientific, Pittsburgh, PA) and used without further purification. Products of synthesis were purified chromatographically on silica gel columns. High-performance liquid chromatography (HPLC) was performed on a system fitted with a photodiode array detector (model 600, Waters Corp, Milford, MA). ^{1}H NMR spectroscopy was performed at 300 MHz (QE-300, General Electric, Fairfield, CT) or 500 MHz (INOVA 500, Varian, Inc., Palo Alto, CA). Analysis of compounds by high-resolution fast-atom-bombardment (FAB) mass spectrometry was performed by the facility in the Department of Biochemistry at Michigan State University (East Lansing, MI). Melting points were obtained on a Mel-Temp II apparatus (Laboratory Devices, Holliston, MA) and are uncorrected. Absorption spectra were acquired on a UV−visible spectrophotometer (Cary 300, Varian, Inc.). Steady-state photolysis of samples was achieved with the multiline UV emission of an argon ion laser (BeamLok 2065-7S, Spectra Physics). We expected that, in cellular experiments, the highly lipophilic caged vanilloids would partition into biomembranes, which represent a hydrophobic but polar environment. Therefore, for all spectroscopic studies, the caged compounds were dissolved in acetonitrile, a nonreactive, polar, aprotic organic solvent.

N-(2-Nitrobenzyl)-vanillylamine Hydrochloride and Free Base (4). Vanillylamine hydrochloride (3.81 g, 19.7 mmol, 1.05 equiv; Aldrich, Milwaukee, WI), 2-nitrobenzaldehyde (2.89 g, 18.8 mmol, 1.0 equiv; Aldrich), and sodium acetate (1.66 g, 20.3 mmol) were dissolved in 1,2-dichloroethane (20 mL) and magnetically stirred for 1 h under nitrogen. Na-

$(CH_3CO_2)_3BH$ (6.27 g, 28 mmol, 1.5 equiv; Aldrich) was then added in one portion. The reaction mixture was stirred overnight (ca. 18 h), diluted with 50 mL of CH_2Cl_2, and quenched with 20 mL of saturated $NaHCO_3$ solution. The organic phase was separated and washed twice with 15-mL portions of saturated $NaHCO_3$ solution. The organic phase was acidified by addition of 10% HCl until the pH of the aqueous phase was ∼2 and then chilled in an ice−water bath for 30 min, whereupon the yellow hydrochloride salt formed. The product was filtered and washed with 20 mL of diethyl ether to yield a light yellow crystalline solid (3.48 g, 57%), mp 196 °C (dec). The hydrochloride salt (0.108 g, 0.33 mmol) was suspended in a mixture of water (1 mL) and CH_2-Cl_2 (5 mL) and stirred at room temperature for 10 min. Saturated $NaHCO_3$ (1 mL) was added, and stirring was continued for 30 min. The organic phase was separated, washed with brine (2 mL), and dried over anhydrous $MgSO_4$. After solvent removal, the free base was obtained as a pale yellow oil. ^{1}H NMR (500 MHz, DMSO-d_6) δ: 3.54 (s, 2H), 3.73 (s, 3H), 3.88 (s, 2H), 6.60−6.70 (m, 2H), 6.86 (s, 1H), 7.48 (t, 1H), 7.63−7.73 (m, 2H), 7.88 (d, 1H, $J = 7.8$ Hz), 8.73 (s, 1H). HRMS: $C_{15}H_{16}N_2O_4$, m/z [M$^+$ + H], calculated 289.1188, found 289.1186.

N-(4-Hydroxy-3-methoxybenzyl)-N-(2-nitrobenzyl)-nonanoylamide or N-(2-Nitrobenzyl)-N-vanillyl-nonanoylamide (Nb-VNA, 1). To a mixture of *N*-(2-nitrobenzyl)vanillylamine hydrochloride (3.25 g, 10 mmol), K_2CO_3 (1.38 g, 10 mmol), and triethylamine (1.52 g, 2.09 mL, 15 mmol) in dry CH_2-Cl_2 (20 mL) was added nonanoyl chloride (2.03 g, 2.07 mL, 11.5 mmol, Aldrich) in one portion with magnetic stirring under nitrogen. The reaction mixture was heated to 50 °C and stirred for 2 h until thin-layer chromatography showed only one spot (hexanes−ethyl acetate, 1:1), whereupon the mixture was washed with saturated $NaHCO_3$ (2 × 25 mL) and brine (2 × 25 mL) and then dried over anhydrous Na_2-SO_4. After flash chromatography on silica gel (hexanes−ethyl acetate, 95:5, then 80:20) and recrystallization from hexane, an off-white powder was obtained (2.4 g, 56%), mp 72−73.5°C. A feature common to the ^{1}H NMR spectra of

compound **1** (Nb-VNA) and compound **2** (Nv-VNA) is noteworthy. Resonance stabilization of the amide bond, together with steric hindrance to rotation about the amide bond, gives rise to cis and trans isomers in relative abundances of $\sim^1/_3$ and $\sim^2/_3$, respectively. The sterically constrained moieties in these two populations, e.g., the benzylic methylenes and the methylene α to the amide carbonyl, give rise to corresponding proton NMR resonances whose integrations reflect the relative isomeric abundances. ^{1}H NMR (300 MHz, CDCl$_3$) δ: 0.87 (t, 3H), 1.25 (m, 10H), 1.68 (m, 2H), 2.27 (t, $^2/_3 \times$ 2H), 2.50 (t, $^1/_3 \times$ 2H), 3.85 (s, 3H), 4.47 (s, $^1/_3 \times$ 2H), 4.52 (s, $^2/_3 \times$ 2H), 4.84 (s, $^2/_3 \times$ 2H), 4.94 (s, $^1/_3 \times$ 2H), 5.62 (br. s, 1H), 6.50−6.95 (m, 3H), 7.30−7.75 (m, 3H), 7.96 (d, $^1/_3 \times$ 1H, $J = 7.6$ Hz), 8.13 (d, $^2/_3 \times$ 1H, $J = 7.6$ Hz). HRMS: C$_{24}$H$_{32}$N$_2$O$_5$, m/z [M$^+$], calculated 428.2311, found 428.2304.

N-(4,5-Dimethoxy-2-nitrobenzyl)vanillylamine (5). Dry DMF (3 mL) and dry acetonitrile (12 mL) were added to a mixture of vanillylamine hydrochloride (0.80 g, 4.22 mmol, Aldrich) and 4,5-dimethoxy-2-nitrobenzyl bromide (1.16 g, 4.22 mmol, Aldrich). As the mixture was stirred at 0 °C under dry N$_2$, 1,2,2,6,6-pentamethylpiperidine (1.32 g, 1.53 mL, 8.44 mmol) was added. Stirring was continued for 1 h at 0 °C and for a further 17 h at room temperature until the nitrobenzyl bromide was completely consumed. The reaction mixture was concentrated under reduced pressure and chromatographed on a silica gel column (hexanes−ethyl acetate, 90:10, then 65:35 + 1% triethylamine). The desired fractions were pooled and evaporated to give a yellow oil (0.95 g, 64.6%). ^{1}H NMR (500 MHz, DMSO-d_6) δ: 3.56 (s, 2H), 3.72 (s, 3H), 3.81 (s, 3H) 3.86 (s, 3H), 3.89 (s, 2H), 5.68 (br. s, 1H), 6.66 (s, 2H), 6.87 (s, 1H), 7.28 (s, 1H), 7.55 (s, 1H). HRMS: C$_{17}$H$_{20}$N$_2$O$_6$, m/z [M$^+$ + H], calculated 349.1400, found 349.1397.

N-(4-Hydroxy-3-methoxybenzyl)-N-(4,5-dimethoxy-2-nitrobenzyl)-nonanoylamide, or N-(2-Nitroveratryl)-N-vanillyl-nonanoylamide (Nv-VNA, 2). To a stirred mixture of *N*-(4,5-dimethoxy-2-nitrobenzyl)vanillylamine (0.89 g, 2.6 mmol), K$_2$CO$_3$ (358 mg, 2.6 mmol), and triethylamine (0.52 g, 0.73 mL) in 10 mL of dry CH$_2$Cl$_2$ under dry nitrogen was added nonanoyl chloride (465 mg, 0.474 mL, 2.63 mmol, Aldrich) in one portion. The reaction mixture was magnetically stirred at room temperature for 2 h until only a single spot could be seen by thin-layer chromatography (hexanes−ethyl acetate, 3:1). The reaction mixture was washed with saturated NaHCO$_3$ (2 × 25 mL) and brine (2 × 25 mL) and dried over anhydrous Na$_2$SO$_4$. Flash chromatography on silica gel (hexanes−ethyl acetate, 95:5, then 80:20) followed by concentration of desired fractions yielded a viscous oil (0.86 g, 69.2%). ^{1}H NMR (500 MHz) δ: 0.87 (t, 3H), 1.2−1.42 (m, 10H), 1.68 (m, 2H), 2.25 (t, $^2/_3 \times$ 2H), 2.50 (t, $^1/_3 \times$ 2H), 3.80−4.00 (m, 9H, methoxys), 4.47 (s, $^1/_3 \times$ 2H), 4.55 (s, $^2/_3 \times$ 2H), 4.90 (s, $^2/_3 \times$ 2H), 4.98 (s, $^1/_3 \times$ 2H), 5.68 (br. s, 1H), 6.56−6.72 (m, 2H), 6.78 − 6.90 (m, 2H), 7.58 (s, $^1/_3 \times$ 1H), 7.76 (s, $^2/_3 \times$ 1H). HRMS: C$_{26}$H$_{36}$N$_2$O$_7$, m/z [M$^+$ + H], calculated 489.2601, found 489.2610.

N-(4-Hydroxy-3-methoxybenzyl)-nonanoylamide, or N-Vanillyl-nonanoylamide (VNA, 6). Under protection of a drying tube, *n*-nonanoic acid (3.00 g, 3.31 mL, 19.0 mmol) was refluxed with thionyl chloride (9.02 g, 5.53 mL, 76 mmol) for 1 h. Excess thionyl chloride was removed by distillation, and residual volatile components were removed

under high vacuum to yield nonanoyl chloride as a colorless oil. The nonanoyl chloride was added dropwise to a stirred solution of *N*-hydroxysuccinimide (2.18 g, 19.0 mmol), triethylamine (2.01 g, 2.91 mL, 20.9 mmol), and 4-(dimethylamino)pyridine (0.23 g, 1.90 mmol) in 40 mL of CH$_2$-Cl$_2$, chilled in an ice−water bath. After addition of nonanoyl chloride was complete, the ice−water bath was removed and the reaction mixture was stirred at room temperature overnight. The reaction mixture was washed with 2 N HCl (60 mL) and brine (2 × 50 mL), dried over anhydrous Na$_2$-SO$_4$, and filtered. Solvent removal under reduced pressure on a rotary evaporator yielded the nonanoic acid *N*-hydroxysuccinimidyl (NHS) ester as an oil which, when placed under high vacuum, became an off-white solid (2.35 g, 49%).

To a mixture of 4-hydroxy-3-methoxybenzylamine hydrochloride (1.25 g, 6.58 mmol) and triethylamine (0.666 g, 0.917 mL, 6.58 mmol) in ethyl acetate (12 mL) maintained under dry argon was gradually added a solution of the NHS ester in 14 mL of ethyl acetate. The suspension was stirred for 48 h. Dry DMF (15 mL) was added to dilute the reaction mixture, and stirring was continued for 24 h under dry argon. The reaction mixture was extracted with 0.5 M sodium citrate buffer (pH 4.5; 3 × 60 mL), washed with water (2 × 50 mL) and brine (50 mL), dried over anhydrous Na$_2$SO$_4$, and filtered. Solvent removal on a rotary evaporator yielded an oil. After chromatographic purification on silica gel (hexanes−ethyl acetate, 2:1), *N*-vanillyl-nonanoylamide (**6**) was obtained as a white solid (1.37 g, 71%). ^{1}H NMR (500 MHz, CDCl$_3$) δ: 0.87 (t, 3H), 1.2−1.35 (m, 10H), 1.65 (m, 2H), 2.19 (t, 2H), 3.88 (s, 3H), 4.36 (d, 2H), 5.64 (br. s, 1H), 6.76 (d, 1H, $J = 8.3$ Hz), 6.81 (s, 1H), 6.86 (d, 1H, $J = 8.1$ Hz).

N-(4-Hydroxy-3-methoxybenzyl)-N-(4,5-dimethoxy-2-nitrobenzyloxycarbonyl)-nonanoylamide, or N-(2-Nitroveratryloxycarbonyl)-N-vanillyl-nonanoylamide (Nvoc-VNA, 3). A stirred solution of *N*-vanillyl-nonanoylamide (0.100 g, 0.341 mmol) in dry CH$_2$Cl$_2$ was maintained under dry argon and chilled on ice. 4,5-Dimethoxy-2-nitrobenzyl chloroformate (0.282 g, 1.02 mmol) and triethylamine (0.103 g, 143 μL) were then added, and the reaction was allowed to proceed 1.5 h, at which time thin-layer chromatography confirmed complete consumption of the starting amide. The reaction mixture was concentrated under reduced pressure to <0.1 mL, suspended in minimal hexanes−ethyl acetate (6:4), and chromatographed on silica gel (hexanes−ethyl acetate, 6:4, then 4.5:5.5). Nvoc-VNA was obtained as a very pale yellow solid (0.164 g, 91%). ^{1}H NMR (500 MHz, CDCl$_3$) δ: 0.87 (t, 3H), 1.2−1.36 (m, 10H), 1.66 (m, 2H), 2.22 (t, 2H), 3.82 (s, 3H), 3.98 (S, 3H), 4.02 (s, 3H), 4.43 (2, 2H), 5.69 (b, 1H), 5.71 (s, 2H), 6.86 (dd, 1H, $J = 7.9$, 2.0 Hz), 6.93 (d, 1H, $J = 2.0$ Hz), 7.10 (d, 1H, $J = 8.3$ Hz), 7.17 (s, 1H), 7.77 (s, 1H).

Quantum Yield Determination

The quantum yield for the photochemical reactions of Nb-VNA and Nv-VNA were determined by a method based on HPLC analysis (*13*). The photorelease reaction is characterized by simple 1:1 stoichiometry between the caged starting material and the released product: molar loss of the starting material by photolysis and the molar product release are

equivalent. To quantitate disappearance of starting caged compound, equal amounts of 4-nitrophenol were added as an internal standard to irradiated samples and to unirradiated controls. In the HPLC traces of these samples, the ratio of the areas of the peaks corresponding to the starting material and the internal standard was determined. From this, the loss of the starting material on photolysis was calculated. Potassium ferrioxalate actinometry was used to measure the light intensity used for photolysis (*14*).

Flash Photolysis Kinetics

A solution of caged vanilloid in a fused silica cuvette was positioned in a flash photolysis kinetic spectrophotometer (LP920, Edinburgh Instruments, Livingston, U.K.) and was magnetically stirred at room temperature. Samples were equilibrated with air except in experiments where an indicator was used to measure photolytically induced pH changes, when the sample was purged with argon and sealed. Photolysis of the sample was effected by an 8.6-ns (fwhm), 200-mJ pulse of 355-nm third harmonic light from a Nd: YAG laser (Quanta-Ray GCR-18S, Spectra Physics, Mountain View, CA). A pair of harmonic separators was used to remove residual fundamental (1064 nm) and second harmonic (532 nm) laser emissions from the photolysis beam. A probe beam from a stabilized xenon arc lamp was focused such that the focal point coincided with the region in the sample where maximal photolysis occurred. The spectrum of the probe beam was obtained through a monochromator. Modulation of the probe beam intensity by a transient photochemical intermediate species was monitored at a chosen wavelength by a fast photomultiplier tube. The intensity-vs-time profile was converted to an absorbance-vs-time trace. Nonlinear least-squares analysis allowed exponential decay times to be extracted from the data. Data in the initial 50-ns window contain artifactual contributions from scattering of the laser pulse and instabilities in the high-sensitivity detection circuitry, and are not included in data analysis.

Loading of Dissociated Neurons with Fluorescent Ca^{2+} Indicator

Dorsal root and nodose ganglia were dissected from adult male rats (Sprague−Dawley, 200−300 g) and dissociated as previously described (*15*). Acutely dissociated dorsal root ganglion (DRG) or nodose ganglion neurons, plated onto poly-D-lysine-coated No. 1 glass coverslips, were loaded with fluo-3 indicator by incubation with 1 μM fluo-3/AM in Leibovitz's L15 medium containing 10% heat-inactivated fetal bovine serum for 60 min at room temperature. During experiments, each coverslip bearing neurons was mounted in a flow chamber and superfused with Locke solution containing (in mM) 136 NaCl, 5.6 KCl, 1.2 NaH$_2$PO$_4$, 1.2 MgCl$_2$, 14.3 NaHCO$_3$, 2.2 CaCl$_2$, 10 mM glucose, equilibrated with 5% CO$_2$/95% O$_2$, at room temperature (21−22 °C). Nominally Ca^{2+}-free Locke solution was prepared by omitting CaCl$_2$ from the formulation. When appropriate, caged vanilloid (1 μM) and capsazepine (5 μM) were applied via the superfusate.

Wide-Field Fluorescence Microscopy and UV Laser Flash Photolysis

For wide-field imaging microscopy, neurons were examined on an inverted microscope (TE200, Nikon) equipped with a UV-transmitting objective (SuperFluor, 40×, N.A. 1.4, Nikon). Intracellular fluo-3 was excited by 488-nm light from a monochromator (PolyChrome II; TILL Photonics, Gräfelfing, Germany) and imaged with a cooled CCD camera (CoolSnap HQ, Roper Scientific, Tucson, AZ). Metafluor software (Universal Imaging, Downingtown, PA) was used for instrument control and data analysis. For photolysis, the multiline UV output (∼375 mW, 333−364 nm) of an argon ion laser (BeamLock 2065-7S; Spectra Physics) was launched into a 100-μm diameter silica optical fiber (Oz Optics, Ontario, Canada). The distal end of the fiber was fitted with a microlens assembly to allow focusing of the transmitted light into a 0.6 mm diameter spot; power at the focal plane was 200 mW. Laser pulses of 20-ms duration were delivered by gating the laser output with a shutter (NM Laser Products, Sunnyvale, CA), resulting in UV exposure of 14 μJ/μm^2 at the specimen.

Recording of Currents Evoked by Photolysis of Caged Vanilloids in Neurons

In focal photolysis experiments, the whole-cell configuration of the patch clamp technique was used to measure membrane currents. Patch pipets (1.5−2.5 MΩ) were fabricated from borosilicate glass stock (World Precision Instruments, Sarasota, FL) on a Flaming-Brown P97 micropipet puller (Sutter Instrument Co., Novato, CA) and connected to an Axopatch 200B amplifier (Axon Instruments, Union City, CA). Data acquisition through the Digidata 1200 interface was controlled with pClamp 8 software (Axon Instruments). Patch pipets contained (in mM) 152 KCH$_3$-SO$_3$, 10.0 HEPES, 2.0 MgCl$_2$, 1.0 Na$_3$ATP, 1.0 Na$_3$GTP, 1.0 KCl, and 50 μM K$_5$Fluo-3 and 10 μM CaCl$_2$. Nodose neurons supported on glass coverslips were loaded with fluo-3 indicator as described above, and incubated for ∼7 min with 5 μM of either Nb-VNA or Nvoc-VNA immediately before the coverslips were loaded into the recording chamber mounted on a laser scanning microscope (LSM 5 Live, Zeiss, Jena, Germany) fitted with a UV-transmitting objective (Plan-Neofluar, 40×, N.A. 1.3, Zeiss). Neurons were then immediately superfused with physiological saline solution that contained (in mM) 120 NaCl, 3.0 KCl, 1.0 NaH$_2$PO$_4$, 25.0 NaHCO$_3$, 1.5 MgCl$_2$, 2.2 CaCl$_2$, and 10 glucose, equilibrated with 95% O$_2$/5% CO$_2$ at 22 °C. After a gigaohm seal (>1.0 GΩ) was formed, the whole-cell configuration was established with neurons voltage-clamped to −55 mV; data were acquired at 5 kHz (1 kHz filter). Membrane input resistance and capacitance were determined from current transients elicited by 5-mV depolarizing voltage steps from the holding potential. Neurons were considered suitable for study if the input resistance was >150 MΩ and the holding current was <200 pA.

For focal photolysis, the 355-nm output of a frequency-tripled Nd:YVO4 laser (30 kHz pulse rate; Series 3500, DPSS Lasers, Santa Clara, CA) is coupled into the microscope through a fiberoptic spot illumination assembly (Rapp OptoElectronic, Hamburg, Germany) to form a 10-μm spot in the specimen plane. In all experiments, the photolysis spot was positioned over the edge of a nodose neuron (typical diameter, 35−50 μm), so that less than one-half of the spot overlapped the neuron (see Supplemental Figure 1, Supporting Information). The laser power at the specimen was 17 mW. To achieve photolysis, a 5-ms light pulse was delivered;

total UV exposure was 1.1 $\mu J/\mu m^2$. Light pulse duration was controlled by gating the laser Q-switch with TTL signals. Electrophysiological data acquisition, imaging, and laser gating were synchronized through a multichannel stimulator (Pulsemaster, World Precision Instruments).

In wide-field photolysis experiments, standard intracellular recording techniques were used to monitor electrical activity. Intracellular micropipets (80−100 MΩ when filled with 3 M KCl) were fabricated from borosilicate glass stock on a Flaming-Brown P-97 micropipet puller (Sutter Instrument Co.). Voltage-clamp recordings were made with an Axo-clamp-2A amplifier (Axon Instruments) in discontinuous mode (sample rate, 8 kHz; 3 kHz filter). Rat nodose neurons on coverslips were mounted in a recording chamber on an inverted microscope (TE200, Nikon) and were superfused with Locke solution containing 1 μM Nb-VNA, Nv-VNA, or Nvoc-VNA. Neurons were accepted for study only if they showed a stable resting membrane potential (<−50 mV) throughout the experiment, and an action potential overshoot >0 mV. During photolysis, the neurons were held at −60 mV. For photolysis, the output of a mercury arc lamp was filtered through UG1 glass and directed through the objective (SuperFluor, 40×, N.A. 1.4, Nikon) to illuminate a 530-μm diameter spot; power at the specimen was 44 mW. An electromechanical shutter (Uniblitz, Vincent Associates, Rochester, NY) was used to give 100-ms flashes. Exposure at the specimen was 20 $\mu J/\mu m^2$. Acquisition of electrophysiological data through the Digidata 1200 interface and subsequent data analysis were performed through pClamp 8 software (Axon Instruments).

Confocal Microscopy and 2-Photon Photolysis

Dissociated neurons were examined on a laser scanning confocal microscope (LSM 510 NLO, Zeiss, Jena, Germany) equipped with an IR-transmitting objective (40×, N.A. 0.9) for 2-photon excitation with a titanium:sapphire (Ti:S) laser (Mira 900F; Coherent, Inc., Santa Clara, CA). Caged vanilloid (5 μM) and capsazepine (5 μM) were included in the bathing medium when appropriate. Fluo-3 was excited with 488-nm emission from an argon ion laser. Each image consisted of 512 by 512 pixels (pixel size 0.22 by 0.22 μm), scanned with a dwell time of 1.6 μs per pixel. For 2-photon photolysis, the 720-nm output (~120-fs pulses) of the Ti:S laser was delivered by the confocal scan head to a region of interest (ROI) within the specimen. Gating and intensity of the Ti:S output were controlled through an acousto-optic modulator (AOM). Total output power of the Ti:S laser at 720 nm was 171 mW before passage through the confocal scan head and 32 mW at the specimen. For photolysis experiments, only ≤20% of total power was used (<6.4 mW at the specimen). During photolysis, the laser was rapidly scanned across the entire cell 10 times, resulting in exposure of ~100 nJ per pixel, or ~2 $\mu J/\mu m^2$.

Data Reduction and Representation

In every fluo-3 fluorescence image acquired, a region of interest (ROI) was defined to enclose each neuron under study. The average pixel intensity (F) in each ROI was calculated. Changes in $[Ca^{2+}]_i$ are presented as the fractional change in intensity relative to the baseline ($\Delta F/F_0$). Baseline intensity (F_0) was defined as the average F for all images

acquired prior to photolysis. Origin software (OriginLab Corp., Northampton, MA) was used for nonlinear least-squares analysis. Numerical results are reported as mean ± SE. Statistically, $p < 0.05$ is considered significant.

RESULTS

In designing a photoreleasable ligand for the vanilloid receptor, we first considered caging capsaicin, which is an amide formed between vanillylamine and 8-methyl-6-non-enoic acid (Figure 1). While the amine is commercially available, the acid is not, which implies additional synthetic complexity. Fortunately, extensive structure−activity studies have shown that vanillylamides with potential agonist activity can be prepared from any of a range of unbranched long-chain fatty acids, with nonanoic acid being optimal (*16*). Thus, *N*-vanillyl-nonanoylamide (VNA; Figure 1) is essentially equipotent with capsaicin in cellular and tissue assays (*4*) and is an easily accessible target for caging. Caging entails attaching a photolabile protective group to VNA so that its activity is abolished until the protective group, or cage, is removed by photolysis. It is known that the hydrogen on the amide nitrogen is necessary for vanilloid activity: replacing the hydrogen with a bulkier substituent abolishes activity (*17*). Moreover, endogenous amide hydrolases do not readily cleave fatty acyl tertiary amides, i.e., those with two substitutions on the amide nitrogen (*18*). Thus, attaching the cage to the amide nitrogen of VNA should generate a caged molecule that is both biologically inactive and resistant to enzymatic degradation. We chose two common photolabile protective groups to attach to the nitrogen of VNA: 2-nitrobenzyl (Nb) and 4,5-dimethoxy-2-nitrobenzyl, which is also known as 2-nitroveratryl (Nv). The two caged vanilloids, Nb-VNA and Nv-VNA (Figure 1), were synthesized following the schemes outlined in Figure 2A and Figure 2B. Detailed synthetic procedures are described in Materials and Methods. These caged vanilloids are lipophilic; therefore, when applied through the extracellular aqueous medium, they are expected to permeate cellular membranes with ease.

While the present project was being completed, two relevant publications appeared. One reported synthesis of model compounds suggesting the feasibility of attaching a cage to the phenolic hydroxyl group of vanilloids (*19*). A second reported the preparation of a caged capsaicin where a nitroveratryloxycarbonyl (Nvoc) group was attached to the phenolic oxygen of the vanillyl moiety of capsaicin (*20*).[3] The same authors also showed that Nvoc-caged capsaicin can be photoreleased to activate heterologously expressed TRPV1 channels in cultured hippocampal neurons, which consequently fired action potential bursts (*20*). Our own experience has shown that caging on phenolic oxygen and, even more so, attaching the cage via an oxycarbonyl linkage tend to result in caged molecules with slower photorelease kinetics (*21−23*). Nevertheless, for comparison, we also prepared an analogously caged VNA in which the Nvoc group was attached to the phenolic oxygen (Figure 1, Figure 2C).

The process whereby VNA is generated photochemically from Nb-VNA or Nv-VNA is represented in Figure 3A. The

---

[3] In ref 13, the abbreviation "DMNB" was used to designate the Nvoc group.
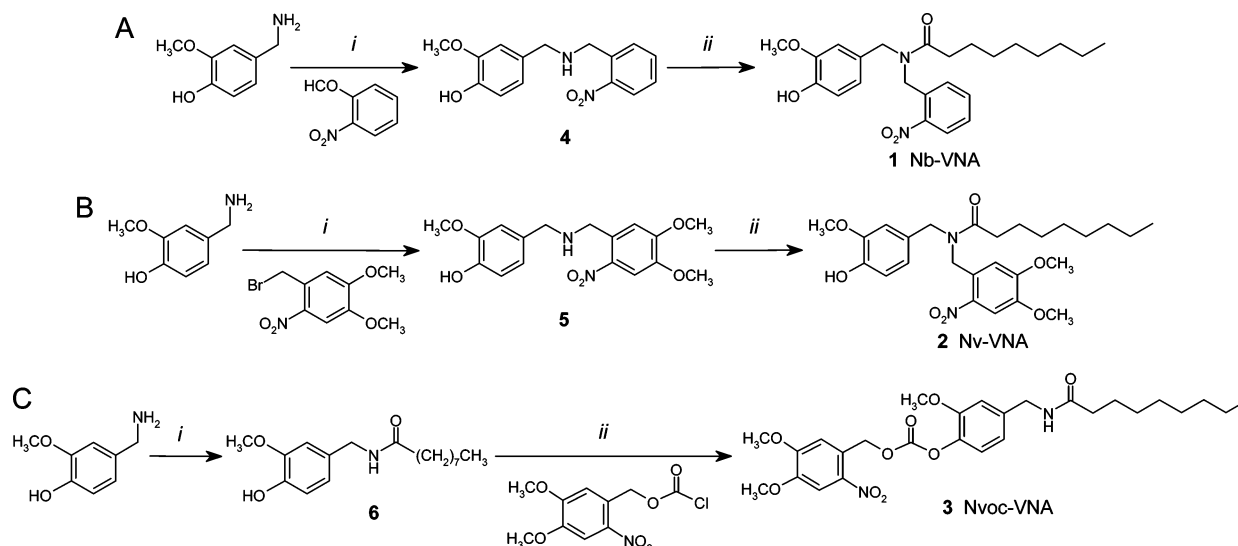
FIGURE 2: Synthetic schemes for the caged vanilloids, Nb-VNA, Nv-VNA, and Nvoc-VNA. Reaction conditions: (A) (i) Na(CH₃CO₂)₃-BH, NaOAc, 1,2-dichloroethane; (ii) K₂CO₃, Et₃N, dichloromethane. (B) (i) 1,2,2,6,6-pentamethylpiperidine, DMF/acetonitrile; (ii) K₂CO₃, Et₃N, dichloromethane. (C) (i) *n*-Nonanoic acid *N*-hydroxysuccinimidyl ester, Et₃N, EtOAc/DMF; (ii) Et₃N, dichloromethane.

UV–visible absorption spectra of Nb-VNA and Nv-VNA before and after photolysis are shown in Figure 3B. Corresponding spectra for Nvoc-VNA are similar to those of Nv-VNA and are available as Supporting Information. The quantum efficiency for photorelease of VNA upon photolysis was $Q = 0.130 \pm 0.002$ ($n = 3$) for Nb-VNA and $Q = 0.0414 \pm 0.0002$ ($n = 3$) for Nv-VNA. In contrast, the quantum efficiency for Nvoc-VNA was much lower at $Q = 0.0049 \pm 0.0004$ ($n = 3$). To investigate the kinetics of photolysis, we used transient absorption spectroscopy to monitor the photolytically generated, short-lived *aci*-nitro intermediate (see Figure 3A) (24–27), whose decay is commonly taken to be concomitant with cleavage of the caging group and release of product (28, 29). Flash kinetic spectroscopy traces for Nb-VNA and Nv-VNA are shown in Figure 3C. Upon flash photolysis with an 8.6-ns pulse of 355-nm UV light, Nb-VNA photolysis displayed a double-exponential time course, with exponential time constants[4] $\tau_1 = 3.47 \pm 0.05$ μs and $\tau_2 = 15.3 \pm 0.1$ μs ($n = 5$ kinetic traces); these two components correspond to 34% and 66% of the total transient absorbance change, respectively. These results indicate that, upon flash photolysis of Nb-VNA, VNA photorelease is 95% complete in <40 μs. The existence of two kinetic components likely reflects geometric isomerism in the *aci*-nitro intermediate: the stereochemical configuration around the enamine double bond (marked by an arrowhead in Figure 3A) can be either *E* or *Z*. Nv-VNA photolysis proceeds somewhat more slowly, exhibiting exponential time constants of $\tau_1 = 19.3 \pm 2.1$ μs and $\tau_2 = 71 \pm 58$ μs ($n = 25$ kinetic traces); these two components account for 71% and 29% of the total transient absorbance change, respectively. Thus, flash photorelease from Nv-VNA is 95% complete in ~125 μs.

Photolysis of Nvoc-VNA proceeds by a somewhat more complex mechanism. Photolysis generated the *aci*-nitro intermediate, which, as monitored by transient absorption spectroscopy, decayed rapidly with a single-exponential time constant of $\tau = 0.297 \pm 0.001$ μs ($n = 5$ kinetic traces; see

Supporting Information). Photolytic cleavage of the nitro-veratryl group from Nvoc-VNA does not liberate VNA directly, but rather the VNA-carbonate ester, which must undergo decarboxylation to yield free VNA, with unimolecular rate constant, k_{dec} (scheme in Figure 3D). The decarboxylation, which is expected to be rate-limiting, cannot be directly observed by optical spectroscopy; however, indirect monitoring is possible. As shown in Figure 3D, decarboxylation of VNA-carbonate to yield carbon dioxide and VNA requires proton uptake; the resulting alkalinization could be monitored indirectly with a pH indicator. The absorbance change of Phenol Red indicator after flash photolysis of Nvoc-VNA is shown in Figure 3D. The absorbance change comprises two exponential components. The slower component has $\tau = 3.5 \pm 1.3$ ms (3 determinations, each with $n = 6$–7 kinetic traces) and is the result of movement of photolyzed material out of, and fresh bulk solution into, the volume defined by the intersection of the photolytic and probe light beams, as a result of mechanical convection in the sample. The time constant of the slow component is indistinguishable from that characteristic of stirring, $\tau = 4.0 \pm 0.4$ ms ($n = 10$ kinetic traces; data not shown). The faster component, attributable to alkalinization consequent to decarboxylation, is characterized by $\tau_{dec} = 270 \pm 40$ μs ($n = 3$ determinations, each with 6–7 kinetic traces).

Published studies on decarboxylation kinetics permit independent estimation of τ_{dec}. Sauers and colleagues determined the rate constants for decarboxylation of 10 monocarbonate esters of alcohols whose pK_as were known (30). Least-squares analysis of the data showed that $-\log \tau_{dec} = \log k_{dec} = (15.55 \pm 0.09) - (1.189 \pm 0.006) \times pK_a$ (see Supporting Information for details). For the phenolic hydroxyl in VNA, standard methods (31, 32) yield an estimate of p$K_a = 10.03$. Therefore, for decarboxylation of VNA-carbonate, we expect $\tau_{dec} = 1/k_{dec} = 240$ μs, which is quite consistent with the experimentally determined value of $\tau_{dec} = 270 \pm 40$ μs. The above results indicate that vanilloid release after photolysis of Nvoc-VNA is expected to be 95% complete after $3\tau_{dec} = 810$ μs. This confirms our earlier

---

[4] Exponential time constant and half-life are related by $t_{1/2} = 0.693\tau$.
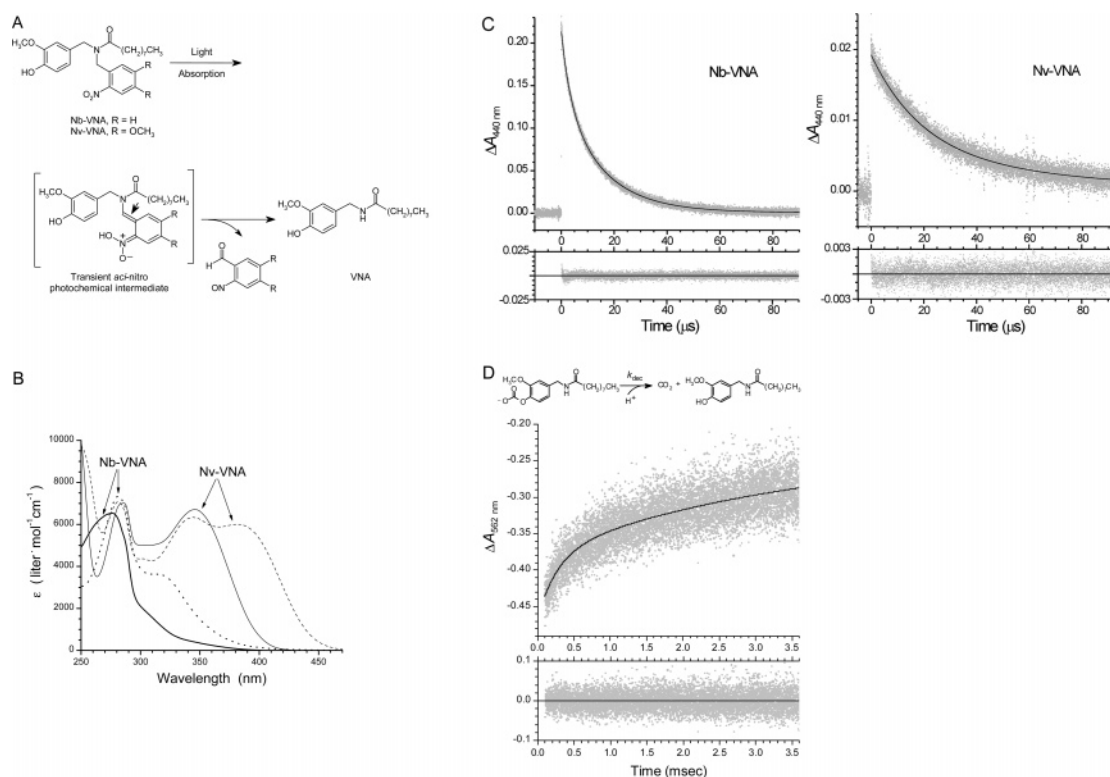
FIGURE 3: Spectroscopic characterization of the photorelease of *N*-vanillylnonanoylamide (VNA) from caged VNA. (A) Photolysis of caged VNA. Light absorption by caged VNA generates the short-lived *aci*-nitro intermediate, which decomposes into the spent cage (a 2-nitrosobenzaldehyde) and VNA. The *aci*-nitro intermediate can exist in two geometric isomeric forms: the configuration around the double bond marked by the arrowhead can be either *E* or *Z*. For the Nb cage, R = H; for the Nv cage, R = OCH$_3$. (B) UV−visible absorption spectra of caged VNAs. Spectra of Nb-VNA acquired before (thick solid line) and after (dotted line) photolysis. Spectra of Nv-VNA acquired before (thin solid line) and after (dashed line) photolysis. Photolysis was for 30 s with 375 mW of the UV emission from an argon ion laser. (C) Transient absorbance spectral changes of Nb-VNA and Nv-VNA following laser flash photolysis. The absorbance at 440 nm of a solution of Nb-VNA or Nv-VNA in acetonitrile was monitored. At time zero, an 8.6-ns pulse of 355-nm light was delivered to the sample. In each case, in the larger panel, gray points are experimental data and the solid black curve is the nonlinear least-squares double-exponential fit to the data; the residuals of the least-squares fit are shown in the smaller lower panel. For Nb-VNA, the two exponential components have time constants $\tau_1 = 3.47 \pm 0.05$ μs and $\tau_2 = 15.3 \pm 0.1$ μs, and account for 34% and 66% of the total transient absorbance change, respectively. For Nv-VNA, the two exponential components have time constants $\tau_1 = 19.3 \pm 2.1$ μs and $\tau_2 = 71 \pm 58$ μs, and account for 71% and 29% of the total transient absorbance change, respectively. Data shown for Nb-VNA are the average of 5 replicate measurements; data shown for Nv-VNA are the average of 25 replicate measurements. Pulse energies were ∼200 mJ and ∼50 mJ for Nb-VNA and Nv-VNA, respectively. (D) Kinetics of decarboxylation of VNA-carbonate monitored indirectly with the pH indicator Phenol Red. Generated by photolysis of Nvoc-VNA, VNA-carbonate, the monocarbonate ester of VNA, undergoes decarboxylation, with proton uptake, to yield carbon dioxide and free VNA. The unimolecular rate constant for decarboxylation is k_{dec}. To monitor decarboxylation kinetics, the absorbance of a solution of Nvoc-VNA (525 μM) in methanol−water (8:2) containing 40 μM Phenol Red indicator was monitored at 562 nm. At time zero, an 8.6-ns, 30-mJ pulse of 355-nm light was delivered to the sample. In the upper panel, gray points are experimental data (average of a total of 20 traces) showing the rising phase of the Phenol Red absorbance signal, and the solid black curve is the nonlinear least-squares double-exponential fit to the data. The two exponential components have time constants $\tau_{slow} = 3.50 \pm 1.29$ ms and $\tau_{fast} = 270 \pm 40$ μs, and correspond to 37% and 63% of the absorbance increase, respectively. The residuals of the least-squares fit are shown in the lower panel. Before the experiment, the sample was adjusted to pH 8.1 and purged with, and sealed under, argon gas.

understanding that attachment of a cage through an oxycarbonyl linkage to an oxygen atom (i.e., a carbonate type linkage) results in a marked slowing of product release after photolysis. The slow photorelease kinetics, together with the 8- to 26-fold lower quantum efficiency relative to Nv-VNA and Nb-VNA, indicate that caging on the phenolic oxygen through a carbonate linkage is far from optimal.

We studied the ability of photoreleased VNA to activate TRPV1 in rat DRG neurons, ∼60% of which are activated by capsaicin (*33, 34*). We used wide-field fluorescence imaging microscopy to monitor the rise in [Ca^{2+}]$_i$ consequent to TRPV1 activation. Shown in Figure 4A are fluorescence traces acquired in two separate experiments from single isolated DRG neurons that had been loaded with the fluorescent Ca^{2+} indicator, fluo-3. When superfused with Locke solution containing 1 μM Nb-VNA, a 20-ms UV pulse evoked a marked rise in [Ca^{2+}]$_i$, as reflected by the increase

in fluo-3 fluorescence intensity. The traces illustrate that there is variability in both the maximal amplitude and the time-to-peak of Ca^{2+} responses from individual neurons. In 6 other neurons, analogous responses were observed. Importantly, prior to superfusion with Nb-VNA, 20-ms UV pulses evoked no response in these neurons (data not shown). These results indicate that the [Ca^{2+}]$_i$ rise evoked by photolysis was dependent on the presence of caged vanilloid, and cannot be attributed to nonspecific cell damage caused by the UV light.

In 30 of 46 DRG neurons examined, VNA photorelease evoked a detectable rise in [Ca^{2+}]$_i$, with the average maximal relative increase in fluo-3 fluorescence, $\Delta F/F_0$, being 0.99 $\pm$ 0.19 ($n = 46$); the data are shown in Figure 4B as a stack plot. In contrast, when VNA was photoreleased onto DRG neurons in the presence of 5 μM capsazepine, a highly selective vanilloid receptor antagonist (*35*), the average
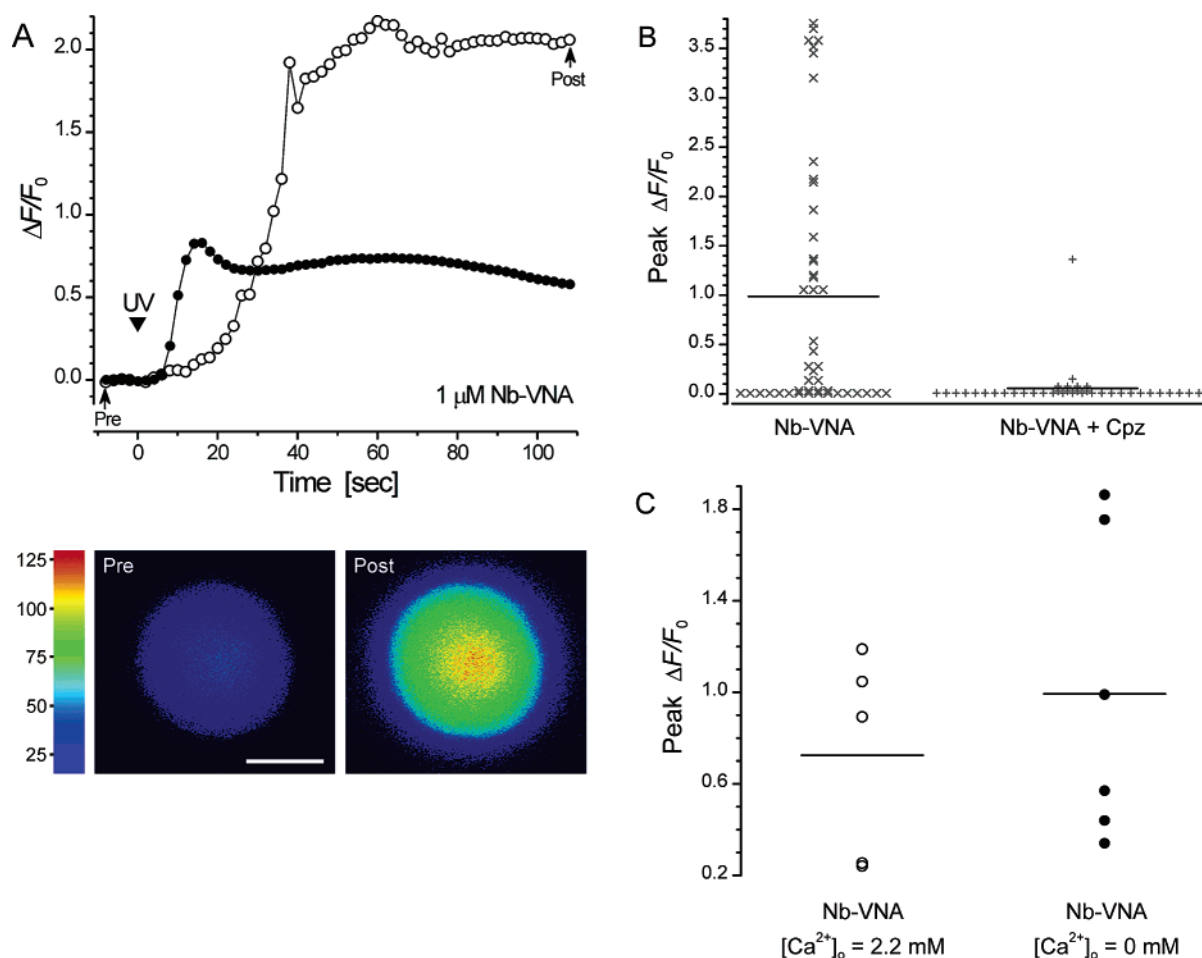
FIGURE 4: $[Ca^{2+}]_i$ signals in DRG neurons in response to in situ UV photolysis of Nb-VNA. (A) In situ photolysis of Nb-VNA evokes robust $[Ca^{2+}]_i$ rises in DRG neurons. Fluorescence traces acquired in two separate experiments from single isolated DRG neurons that had been loaded with the fluorescent Ca^{2+} indicator, fluo-3. Each neuron was superfused for 5 min with Locke solution containing 1 μM Nb-VNA. Thereafter, a 20-ms UV pulse (arrowhead marked "UV") evoked a marked rise in $[Ca^{2+}]_i$, as reflected by the increase in fluo-3 fluorescence. The traces show that both the maximal amplitude and the rise time of the vanilloid-evoked Ca^{2+} response can vary among cells. Representative pre- and postphotolysis confocal fluorescence images of the neuron, corresponding to points in the trace marked by arrows, are shown below the graph. Fluorescence intensity in the images is encoded in pseudocolor. Scale bar = 10 μm. In all experiments shown in Figure 4, UV exposure at the specimen was 14 μJ/μm^2. (B) Capsazepine, a vanilloid receptor antagonist, blocks the $[Ca^{2+}]$ rise in DRG neurons evoked by photolysis of Nb-VNA. In the absence of 5 μM capsazepine (Cpz), UV photorelease of VNA from Nb-VNA evoked detectable $[Ca^{2+}]_i$ rises in the majority of DRG neurons (30 of 46). In the presence of 5 μM capsazepine, only 1 of 39 DRG neurons showed a sizable rise in $[Ca^{2+}]_i$. The data were binned in increments of 0.05 on the $\Delta F/F_0$ scale. Solid horizontal lines indicate the mean peak $\Delta F/F_0$ for each distribution: without Cpz, 0.99 ± 0.19 (n = 46); with Cpz, 0.055 ± 0.035 (n = 39). (C) Photoreleased vanilloid can elevate $[Ca^{2+}]_i$ in the absence of extracellular Ca^{2+}. In normal Locke solution ($[Ca^{2+}]$ = 2.2 mM), UV photorelease of VNA evoked a $[Ca^{2+}]_i$ rise in 5 out of 11 DRG neurons. In Ca^{2+}-free Locke solution, VNA photorelease evoked a $[Ca^{2+}]_i$ rise in 6 out of 14 DRG neurons. Solid horizontal lines indicate the mean peak $\Delta F/F_0$ for each responsive population: in 2.2 mM Ca^{2+}, 0.72 ± 0.20 (n = 5); in Ca^{2+}-free medium, 0.99 ± 0.27 (n = 6).

maximal response was greatly reduced to $\Delta F/F_0$ = 0.055 ± 0.035 (n = 39; Figure 4B). In the presence of capsazepine, only 1 of 39 cells showed a significant $[Ca^{2+}]_i$ rise, while the rest showed extremely feeble response or no response at all. These results confirm that the response of the DRG neurons to photolysis of Nb-VNA was mediated by the TRPV1 receptor.

In a separate series of experiments, we asked if photorelease of VNA in the absence of extracellular Ca^{2+} could evoke responses in DRG neurons. Interestingly, the response to VNA photorelease was not significantly different in Ca^{2+}-free Locke solution (p = 0.466; Figure 4C). In Ca^{2+}-containing medium, 5 of 11 neurons showed a measurable $[Ca^{2+}]_i$ change in response to photoreleased VNA, with peak $\Delta F/F_0$ being 0.72 ± 0.20 (n = 5), while in Ca^{2+}-free medium, 6 of 14 neurons showed detectable response, with peak $\Delta F/F_0$ being 0.99 ± 0.27 (n = 6). These observations

indicate that vanilloids can act to release Ca^{2+} from intracellular stores.

While a $[Ca^{2+}]$ rise is a consequence of TRPV1 activation and serves as a convenient indication of activation, the time course of the $[Ca^{2+}]$ rise does not accurately reflect the activation kinetics of TRPV1 channels. This is because the time course depends on the balance of several factors, such as cellular Ca^{2+} buffering, cellular processes that admit Ca^{2+} into the cytosol (including TRPV1 channels), and processes that remove Ca^{2+} from the cytosol. The kinetics of TRPV1 channel activation by photoreleased vanilloid can be studied directly by measuring the ionic current that flows into the cell as TRPV1 channels open. We compared the inward currents evoked by photorelease of Nb-VNA and Nvoc-VNA in rat nodose ganglion neurons, which are vagal sensory neurons, the vast majority (≥75%) of which are vanilloid-responsive (*36*) (Figure 5). The neurons were incubated with
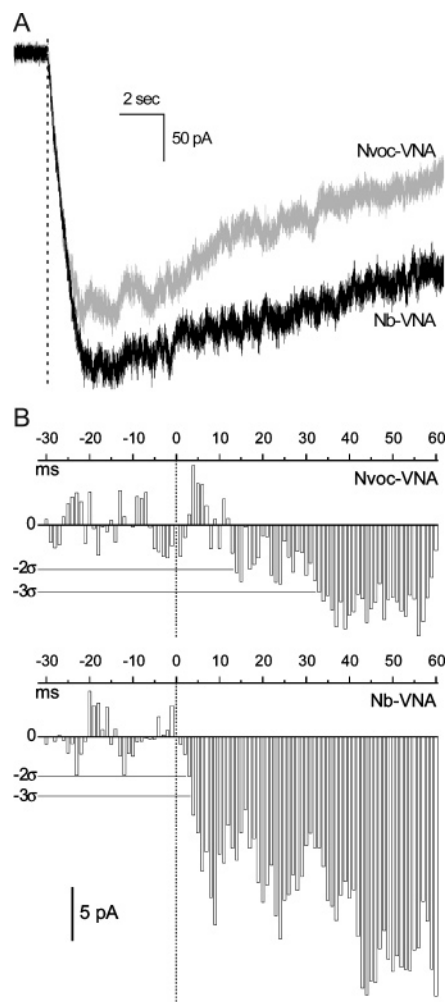
FIGURE 5: Comparison of inward currents activated by photorelease of Nb-VNA and Nvoc-VNA in nodose ganglion neurons. (A) Whole-cell currents recorded in rat nodose ganglion neurons loaded with Nb-VNA (black trace; average of 3 experiments) or Nvoc-VNA (gray trace; average of 2 experiments), and voltage-clamped at −55 mV. Cells were loaded by incubation with 5 μM caged vanilloid for ∼7 min and then superfused with physiological saline. Currents were activated by a 5-ms flash of 355-nm light delivered to a 10-μm spot positioned over the edge of the neuron (typically 35−50 μm in diameter). Photolysis was thus restricted to a small region near the plasma membrane. The dashed line marks the start of the photolytic flash. The UV exposure was 1.1 μJ/μm^2. (B) Time courses of whole-cell currents around the time of photolysis shown at higher resolution. Data from Figure 5A were grouped into 1-ms intervals, and the average current in each interval was plotted as a bar graph against time (upper panel, Nvoc-VNA data; lower panel, Nb-VNA data); vertical dotted lines mark the start of the 5-ms flash. Current levels corresponding to 2 and 3 standard deviations (2σ and 3σ) from baseline are marked by thin horizontal lines in each panel. The current activated by Nvoc-VNA exceeded the 2σ level after 13 ms, and the 3σ level after 32 ms. The current activated by Nb-VNA exceeded both the 2σ and 3σ levels in <4 ms.

caged vanilloid for ∼7 min and then superfused with physiological saline. Ionic currents were recorded in the whole-cell configuration. A 5-ms UV flash was delivered to a 10-μm spot overlapping the edge of the neuron. The inward currents evoked by a 5-ms photolytic flash in neurons loaded with Nb-VNA ($n = 3$) and Nvoc-VNA ($n = 2$) are shown in Figure 5A (black and gray traces, respectively). The current time courses around the time of the flash are shown at higher resolution in Figure 5B, where data from Figure 5A were grouped into 1-ms intervals and the average

current in each interval was plotted as a bar graph against time. It can be seen that the current activated by Nb-VNA photorelease developed more quickly, with current amplitude exceeding 3 standard deviations from baseline in under 4 ms. In contrast, the current activated by Nvoc-VNA developed more slowly, exceeding the 2 and 3 standard deviation levels in 12 and 32 ms, respectively. Finally, we also compared the efficacy of the three caged vanilloids for activating inward current under wide-field photolysis conditions. For these experiments, the nodose ganglion neurons were superfused with Locke solution containing 1 μM caged vanilloid. Currents were recorded through intracellular electrodes. Photolysis was achieved with 100-ms pulses of light from a mercury arc lamp, filtered through UG1 glass to block wavelengths outside the 300−400-nm window. The maximum current amplitudes evoked by photorelease of Nb-VNA, Nv-VNA, and Nvoc-VNA were 145 ± 81 pA ($n = 3$), 164 ± 125 pA ($n = 3$), and 136 ± 33 pA ($n = 3$), respectively. These values are not significantly different. In the absence of caged molecules, no current was activated by the light flash in 5 control neurons.

Because photolysis with UV light can cause uncaging above and below the plane of focus in a sample, albeit at lower levels, 1-photon photolysis may not have sufficient spatial resolution for selective excitation of single neurons in structurally complex and densely innervated preparations. Therefore, we next examined the feasibility of photoreleasing VNA through 2-photon excitation. That is, instead of being photolyzed by absorbing a single UV photon, could Nb-VNA be photolyzed by simultaneously absorbing 2 long-wavelength photons, the sum of whose energies being equivalent to that carried by a single UV photon? Because only in the sub-femtoliter focal volume of a high-numerical-aperture microscope objective is the photon flux sufficiently high to permit 2-photon excitation, stimulation by 2-photon photolysis of caged molecules can be achieved with potentially much higher spatial resolution than is possible with 1-photon excitation. We chose to use the 720-nm output of a mode-locked Ti:S laser: two 720-nm photons are energetically equivalent to one 360-nm photon. We found that although 2-photon photolysis of Nb-NVA was feasible, relatively high excitation light intensities were required (data not shown). Moreover, in whole-tissue preparations, the light intensity required for 2-photon photolysis of Nb-VNA was sufficient to cause cellular damage, as evidenced by rapid changes in neuronal morphology that sometimes occurred in response to irradiation in the absence of caged compound. Therefore, we required a caged vanilloid that can be photolyzed by 2-photon excitation at lower light intensities.

In order for a caged vanilloid to be photoreleasable at lower pulse energies, it must have a higher 2-photon cross section, which is the 2-photon equivalent of the extinction coefficient that characterizes a molecule's ability to absorb single photons. Shifting the UV−visible absorption maximum of the caged molecule to longer wavelengths could improve the efficiency of 2-photon excitation. The spectra in Figure 3B show that the long-wavelength absorption peak of Nv-VNA is red-shifted by ∼70 nm, compared with Nb-VNA. At 360 nm, the extinction coefficient of Nv-VNA is much larger than that of Nb-VNA. Therefore, Nv-VNA should be a better 2-photon absorber at 720 nm than Nb-VNA. Indeed, the Ti:S laser power required to photolyze
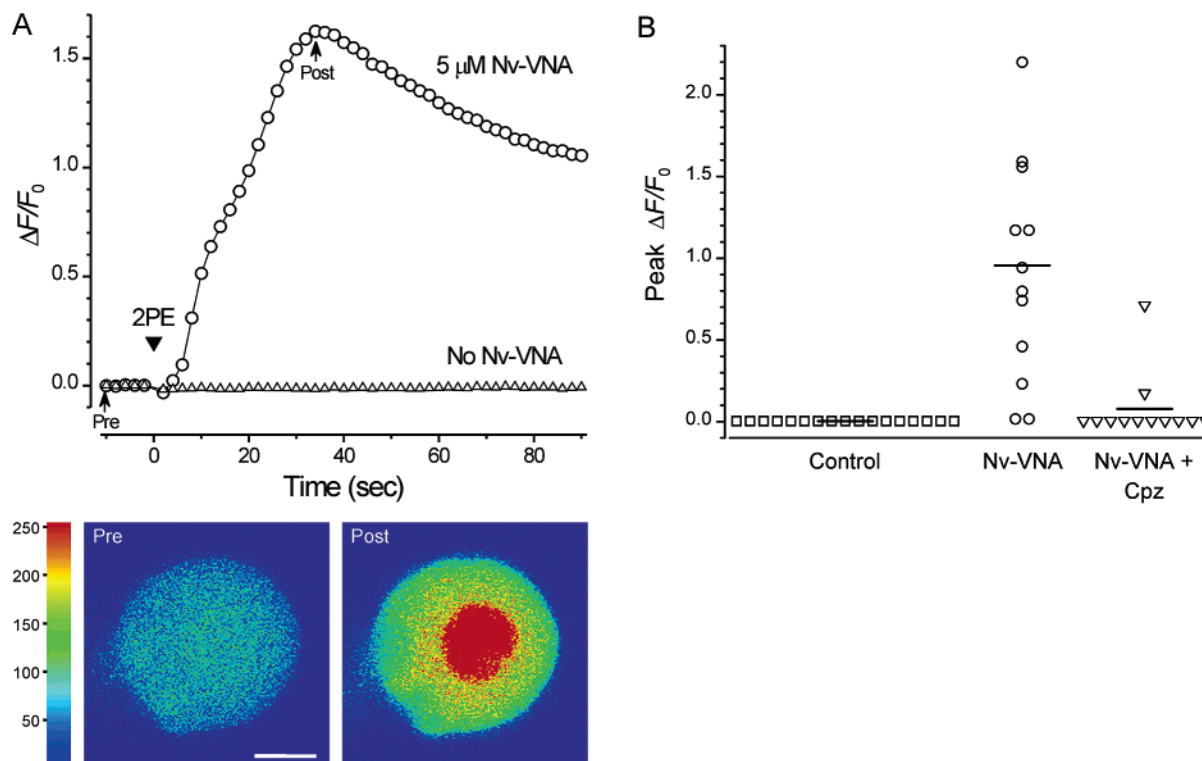
FIGURE 6: Effect of 2-photon photolysis of Nv-VNA on nodose ganglion neurons. (A) In situ 2-photon photolysis of Nv-VNA evokes robust $[Ca^{2+}]_i$ rises in nodose ganglion neurons. Fluorescence traces acquired in two separate experiments from single nodose ganglion neurons that had been loaded with the fluorescent Ca^{2+} indicator, fluo-3. When the neuron was superfused for 5 min with Locke solution containing 5 μM Nv-VNA, scanning 2-photon excitation (arrowhead marked "2PE") evoked a sharp rise in $[Ca^{2+}]_i$ (circles), as reflected by a large increase in fluo-3 fluorescence. In contrast, in a neuron not incubated with Nv-VNA, 2-photon excitation evoked no response (triangles). During 2-photon excitation, the Ti:S laser beam was scanned across the cell 10 times; each pixel (0.22 $\times$ 0.22 μm) received 16 μs of total exposure, corresponding to total exposure of ~100 nJ per pixel, or ~2 μJ/μm^2. Representative pre- and postphotolysis confocal fluorescence images of the responsive neuron, corresponding to points in the trace marked by arrows, are shown below the graph. Fluorescence intensity in the images is encoded in pseudocolor. Scale bar = 10 μm. (B) The $[Ca^{2+}]_i$ rise in nodose ganglion neurons evoked by 2-photon photolysis of Nv-VNA is blocked by capsazepine, a vanilloid receptor antagonist. None of 17 control neurons exposed to the pulsed 720-nm emission from a titanium-sapphire laser in the absence of Nv-VNA showed a $[Ca^{2+}]_i$ response. In the presence of 5 μM Nv-VNA, the same exposure to 720-nm light evoked $[Ca^{2+}]_i$ rises in 12 of 14 neurons. In the presence of 5 μM Nv-VNA *and* 5 μM capsazepine (Cpz, a vanilloid antagonist), the same exposure to 720-nm light triggered a significant response in only 1 out of 11 neurons. Solid horizontal lines indicate the mean peak $\Delta F/F_0$ for each population: control, 0.003 $\pm$ 0.0008 ($n = 17$); in the presence of Nv-VNA, 0.96 $\pm$ 0.17 ($n = 14$); in the presence of Nv-VNA and Cpz, 0.078 $\pm$ 0.0593 ($n = 12$).

Nv-NVA with 2-photon excitation and evoke a biological response in DRG neurons was 5-fold lower than that required for Nb-NVA. Because 2-photon excitation depends on the square of the incident laser power (*37*), this implies a 25-fold improvement in the 2-photon cross section.

We studied the effect of 2-photon photolysis of Nv-VNA on rat nodose ganglion neurons. Exposing nodose ganglion neurons loaded with fluo-3 to 2-photon excitation elicited no response in the absence of Nv-VNA (Figure 6): the mean peak $\Delta F/F_0$ was 0.003 $\pm$ 0.0008 ($n = 17$). In the presence of 5 μM Nv-VNA, 2-photon excitation evoked a robust Ca^{2+} transient in 12 out of 14 cells, with peak $\Delta F/F_0$ being 0.96 $\pm$ 0.17 ($n = 14$). The response to photoreleased VNA was mediated by the vanilloid receptor, because when the experiment was repeated in the presence of the TRPV1 antagonist, capsazepine (5 μM), only 2 out of 12 cells responded feebly, with the mean peak $\Delta F/F_0$ being 0.078 $\pm$ 0.0593 ($n = 12$). These results demonstrate that Nv-VNA is readily photolyzed, through 2-photon excitation by ultrashort pulses of red light, to release VNA.

DISCUSSION

The two caged vanilloid ligands Nb-VNA and Nv-VNA are lipophilic molecules that readily enter cells. In both cases,

the photolabile protective group, or cage, is attached directly to the amide nitrogen of the vanilloid moiety, VNA. These caged molecules can be photolyzed to release active vanilloid ligand with good quantum efficiency and microsecond kinetics. In parallel studies, we determined that although it is synthetically easier to use a one-step reaction to place the Nvoc cage on the phenolic oxygen of the vanilloid, the resulting caged molecule photolyzes with low quantum efficiency and slow product release kinetics in vitro. These findings are consistent with our earlier studies (*21−23*).

When Nb-VNA and Nv-VNA are photolyzed in situ in DRG and nodose ganglion neurons, the photoreleased vanilloid ligands rapidly activate TRPV1 receptors, as evidenced by the resulting capsazepine-inhibitable rise in $[Ca^{2+}]_i$, visualized through fluorescence microscopy in neurons loaded with the fluorescent Ca^{2+} indicator, fluo-3. That photolysis of caged vanilloids in neurons can evoke a large rise in $[Ca^{2+}]_i$ even in the absence of an extracellular source of Ca^{2+} indicates that functional TRPV1 receptors can be activated by the photoreleased vanilloid to mediate Ca^{2+} release from intracellular Ca^{2+} stores. This observation accords with earlier cell biological studies (*38, 39*).

When tested in nodose ganglion neurons for their ability to activate TRPV1 channels to pass inward current, photorelease of Nb-VNA activated an inward current in <4 ms, whereas current activation by photorelease of Nvoc-VNA required 12–32 ms. These activation kinetics are very fast in light of earlier reports that extracellularly applied capsaicin could evoke inward currents in neurons, but with latency-to-activation of at least a few hundred milliseconds (*40, 41*). The latency has been attributed to the need for extracellular capsaicin to cross the plasma membrane in order to access the TRPV1 ligand-binding site, which is intracellular (*42*).

Most importantly, we demonstrated that Nv-VNA can be readily photolyzed through 2-photon excitation at light intensities that are biologically benign. It is interesting to compare Nv-VNA to Bhc-glu (*43*), a caged glutamate that has been shown to be efficacious in 2-photon photostimulation experiments. We can estimate from reported measurements (*43*) that the 2-photon action cross section (i.e., the product of the 2-photon absorption cross section and the quantum efficiency of photorelease) of Bhc-glu is greater than that of Nv-VNA by a factor ≥ 4. That Nv-VNA works well in biological experiments is at least partly due to the fact that vanilloid ligands exhibit high potency at the TRPV1 receptor (*44*). With 2-photon excitation, because photolysis can only occur within the focal volume of the focused light beam (*45*), photorelease on the submicrometer scale can potentially be achieved. Therefore, we expect vanilloid photorelease to be a powerful method for probing peripheral nerve terminals of TRPV1-expressing nociceptive neurons in densely innervated tissue with high temporal and spatial precision. One such tissue is the cornea of the eye, where $\geq 10^6$ nerve terminals, predominantly nociceptive, reside within an epithelial layer that is only 50 μm in thickness (*46, 47*). Experiments using the caged vanilloids to explore the functional properties of corneal nerve terminals are under way.

SUPPORTING INFORMATION AVAILABLE

Positioning of focal photolysis spot in neurons; UV–visible and transient absorption spectroscopy of Nvoc-VNA; quantitative estimation of decarboxylation rate constant of monocarbonate esters. This material is available free of charge via the Internet at http://pubs.acs.org.

REFERENCES

1. Perl, E. R. (1996) Pain and the Discovery of Nociceptors, in *Neurobiology of Nociceptors* (Belmonte, C., and Cervero, F., Eds.) pp 5–36, Oxford University Press, New York.

2. Wood, J. N., Winter, J., James, I. F., Rang, H. P., Yeats, J., and Bevan, S. (1988) Capsaicin-induced ion fluxes in dorsal root ganglion cells in culture, *J. Neurosci. 8*, 3208–3220.

3. Bevan, S. J., and Docherty, R. J. (1993) Cellular Mechanisms of the Action of Capsaicin, in *Capsaicin in* the Study of Pain (Wood, J. N., Ed.) pp 2 –44, Academic Press, London.

4. Walpole, C. S. J., and Wrigglesworth, R. (1993) Structural Requirements for Capsaicin Agonists and Antagonists, in *Capsaicin in the Study of Pain* (Wood, J. N., Ed.) pp 63–81, Academic Press, London.

5. Caterina, M. J., Schumacher, M. A., Tominaga, M., Rosen, T. A., Levine, J. D., and Julius, D. (1997) The capsaicin receptor: a heat-activated ion channel in the pain pathway, *Nature 389*, 816–824.

6. Kaplan, J. H., Forbush, B., III, and Hoffman, J. F. (1978) Rapid photolytic release of adenosine 5′-triphosphate from a protected analogue: Utilization by the Na:K pump of human red blood cell ghosts, *Biochemistry 17*, 1929–1935.

7. Adams, S. R., and Tsien, R. Y. (1993) Controlling cell chemistry with caged compounds, *Annu. Rev. Physiol. 55*, 755–784.

8. Kao, J. P. Y., and Adams, S. R. (1993) Photosensitive caged compounds. Design, properties, and biological applications, in *Optical Microscopy: Emerging Methods and Applications* (Herman, B., and Lemasters, J. J., Eds.) pp 27–85, Academic Press, San Diego.

9. Nerbonne, J. M. (1996) Caged compounds: tools for illuminating neuronal responses and connections, *Curr. Opin. Neurobiol. 6*, 379–386.

10. Marriott, G., and Walker, J. W. (1999) Caged peptides and proteins: new probes to study polypeptide function in complex biological systems, *Trends Plant Sci. 4*, 330–334.

11. Shigeri, Y., Tatsu, Y., and Yumoto, N. (2001) Synthesis and application of caged peptides and proteins, *Pharmacol. Ther. 91*, 85–92.

12. Lawrence, D. S. (2005) The preparation and in vivo applications of caged peptides and proteins, *Curr. Opin. Chem. Biol. 9*, 570–575.

13. de Mayo, P., and Shizuka, H. (1976) Measurements of Reaction Quantum Yields, in *Creation and Detection of Excited States* (Ware, W. R., Ed.) Vol. 4, pp 139–215, Marcel Dekker, Inc., New York.

14. Hatchard, C. G., and Parker, C. A. (1956) A new sensitive chemical actinometer. II. Potassium ferrioxalate as a standard chemical actinometer, *Proc. R. Soc. London, Ser. A 235*, 518–536.

15. Oh, E. J., and Weinreich, D. (2004) Bradykinin decreases K^+ and increases Cl^- conductances in vagal afferent neurones of the guinea pig, *J. Physiol. 558*, 513–526.

16. Walpole, C. S. J., Wrigglesworth, R., Bevan, S., Campbell, E. A., Dray, A., James, I. F., Masdin, K. J., Perkins, M. N., and Winter, J. (1993) Analogues of capsaicin with agonist activity as novel analgesic agents; structure–activity studies. 3. The hydrophobic side-chain "C-region", *J. Med. Chem. 36*, 2381–2389.

17. Walpole, C. S. J., Wrigglesworth, R., Bevan, S., Campbell, E. A., Dray, A., James, I. F., Masdin, K. J., Perkins, M. N., and Winter, J. (1993) Analogues of capsaicin with agonist activity as novel analgesic agents; structure–activity studes. 2. The amide bond "B-region", *J. Med. Chem. 36*, 2373–2380.

18. Lang, W., Qin, C., Lin, S., Khanolkar, A. D., Goutopoulos, A., Fan, P., Abouzid, K., Meng, Z., Biegel, D., Makriyannis, A. (1999) Substrate specificity and stereoselectivity of rat brain microsomal anandamide amidohydrolase, *J. Med. Chem. 42*, 896–902.

19. Katritzky, A. R., Xu, Y.-J., Vakulenko, A. V., Wilcox, A. L., and Bley, K. R. (2003) Model compounds of caged capsaicin: Design, synthesis, and photoreactivity, *J. Org. Chem. 68*, 9100–9104.

20. Zemelman, B. V., Nesnas, N., Lee, G. A., and Miesenböck, G. (2003)Photochemical gating of heterologous ion channels: Remote control over genetically designated populations of neurons, *Proc. Natl. Acad. Sci. U.S.A. 100*, 1352–1357.

21. Muralidharan S., and Nerbonne, J. M. (1995) Photolabile "caged" adrenergic receptor agonists and related model compounds, *J. Photochem. Photobiol. B 27*, 123–137.

22. Rossi, F. M., and Kao, J. P. Y. (1997) Nmoc-DBHQ: A new caged molecule for modulating sarcoplasmic/endoplasmic reticulum Ca^{2+} ATPase activity with light flashes, *J. Biol. Chem. 272*, 3266–3271.

23. Rossi, F. M., Margulis, M., Tang, C.-M., and Kao, J. P. Y. (1997) *N*-Nmoc-glutamate: A new caged glutamate with high chemical stability and low pre-photolysis activity, *J. Biol. Chem. 272*, 32933–32939.

24. Yip, R. D., Sharma, D. K., Giasson, R., and Gravel, D. (1985) Photochemistry of the *o*-nitrobenzyl system in solution: evidence for singlet-state intramolecular hydrogen abstraction, *J. Phys. Chem. 89*, 5328–5330.

25. Schupp, H., Wong, W. K., and Schnabel, W. (1987) Mechanistic studies of the photorearrangement of *o*-nitrobenzyl esters, *J. Photochem. 36*, 85–97.

26. Zhu, Q. Q., Schnabel, W., and Schupp, H. (1987) Formation and decay of nitronic acid in the photorearrangement of *o*-nitrobenzyl esters, *J. Photochem. 39*, 317–332.

27. Yip, R. W., Wen, Y. X., Gravel, D., Giasson, R., and Sharma, D. K. (1991) Photochemistry of the *o*-nitrobenzyl system in solution: identification of the biradical intermediate in the intramolecular rearrangement, *J. Phys. Chem. 95*, 6078–6081.

28. Walker, J. W., Reid, G. P., McCray, J. A., and Trentham, D. R. (1988) Photolabile 1-(2-nitrophenyl)ethyl phosphate esters of

adenine nucleotide analogs. Synthesis and mechanism of photolysis, *J. Am. Chem.* Soc. *110*, 7170−7177.

29. McCray, J. A., and Trentham, D. R. (1989) Properties and uses of photoreactive caged compounds, *Annu. Rev. Biophys. Biophys. Chem. 18*, 239−270.

30. Sauers, C. K., Jencks, W. P., and Groh, S. (1975) The alcohol-bicarbonate-water system. Structure−reactivity studies on the equilibria for formation of alkyl monocarbonates and on the rates of their decomposition in aqueous alkali, *J. Am. Chem. Soc. 97*, 5546−5553.

31. Biggs, A. I., and Robinson, R. A. (1961) The ionisation constants of some substituted anilines and phenols: a test of the Hammett relation, *J. Chem. Soc.* 388−393.

32. Perrin, D. D., Dempsey, B., and Serjeant, E. P. (1981) *pK$_a$ Prediction for Organic Acids and Bases*, Chapman and Hall, London.

33. Winter J. (1987) Characterization of capsaicin-sensitive neurones in adult rat dorsal root ganglion cultures, *Neurosci. Lett. 80*, 134−140.

34. Cardenas, C. G., Del Mar, L. P., and Scrogg, R. S. (1995) Variation in serotonergic inhibition of calcium channel currents in four types of rat sensory neurons differentiated by membrane properties, *J. Neurophysiol. 74*, 1870−1879.

35. Bevan, S., Hothi, S., Hughes, G., James, I. F., Rang, H. P., Shah, K., Walpole, C. J. S., and Yeats, J. C. (1992) Capsazepine: a competitive antagonist of the sensory neurone excitant capsaicin, *Br. J. Pharmacol. 107*, 544−552.

36. Marsh, S. J., Stansfeld, C. E., Brown, D. A., Davey, R., and McCarthy, D. (1987) The mechanism of action of capsaicin on sensory C-type neurons and their axons in vitro, *Neuroscience 23*, 275−289.

37. Boyd, R. W. (2003) *Nonlinear Optics*, 2nd ed., pp 515−532, Academic Press, San Diego.

38. Eun, S. Y., Jung, S. J., Park, Y. K., Kwak, J., Kim, S. J., Kim, J. (2001) Effects of capsaicin on Ca^{2+} release from the intracellular Ca^{2+} stores in the dorsal root ganglion cells of adult rats, *Biochem. Biophys. Res. Commun. 285*, 1114−1120.

39. Liu, M., Liu, M. C., Magoulas, C., Priestley, J. V., Willmott, N. J. (2003) Versatile regulation of cytosolic Ca^{2+} by vanilloid receptor I in rat dorsal root ganglion neurons, *J. Biol. Chem. 278*, 5462−5472.

40. Koplas, P. A., Rosenberg, R. L., and Oxford, G. S. (1997) The role of calcium in the desensitization of capsaicin responses in rat dorsal root ganglion neurons, *J. Neurosci. 17*, 3525−3537.

41. Gunthorpe, M. J., Harries, M. H., Prinjha, R. K., Davis, J. B., Randall, A. (2000) Voltage- and time-dependent properties of the recombinant rat vanilloid receptor (rVR1), *J. Physiol. 525*, 747−759.

42. Jung, J., Hwang, S. W., Kwak, J., Lee, S. Y., Kang, C. J., Kim, W. B., Kim, D., and Oh, U. (1999) Capsaicin binds to the intracellular domain of the capsaicin-activated ion channel, *J. Neurosci. 19*, 529−538.

43. Furuta, T., Wang, S. S., Dantzker, J. L., Dore, T. M., Bybee, W. J., Callaway, E. M., Denk, W., and Tsien, R. Y. (1999) Brominated 7-hydroxycoumarin-4-ylmethyls: photolabile protecting groups with biologically useful cross-sections for two photon photolysis, *Proc. Natl. Acad. Sci. U.S.A., 96*, 1193−1200.

44. Tominaga, M., Caterina, M. J., Malmberg, A. B., Rosen, T. A., Gilbert, H., Skinner, K., Raumann, B. E., Basbaum, A. I., Julius, D. (1998) The cloned capsaicin receptor integrates multiple pain-producing stimuli, *Neuron 21*, 531−543.

45. Williams, R. M., Piston, D. W., Webb, W. W. (1994) Two-photon molecular excitation provides intrinsic 3-dimensional resolution for laser-based microscopy and microphotochemistry, *FASEB J. 8*, 804−813.

46. Zander, E., Weddell, G. (1951) Observations on the innervation of the cornea, *J. Anat. 85*, 68−69.

47. MacIver, M. B., Tanelian, D. L. (1993) Structural and functional specialization of Aδ and C fiber free nerve endings innervating rabbit corneal epithelium, *J. Neurosci. 13*, 4511−4524.